ELSEVIER

Polymer 41 (2000) 1561–1569

polymer

Shear banding in polyamide 6 films as revealed by atomic force microscopy

V. Ferreiro, Y. Pennec, R. Séguéla, G. Coulon*

Université des Sciences et Technologies de Lille, Laboratoire de Structure et Propriétés de l'Etat Solide (associé au CNRS), 59655 Villeneuve d'Ascq Cedex, France

Received 4 January 1999; accepted 26 March 1999

Abstract

Semicrystalline polymers exhibit different levels of microstructure: macromolecules, individual crystalline lamellae, stacks of lamellae separated by amorphous layers, spherulites. Due to such complexity, the understanding of their macroscopic mechanical behaviour requires study of the plastic deformation mechanisms which occur from the nanoscopic to the microscopic scale. We are interested here in the local plastic events which are responsible for the yielding of semicrystalline polymers. Our aim is to show that atomic force microscopy (AFM) is a good tool to image and characterise those mechanisms down to the nanoscopic scale. Polyamide 6 films have been drawn just beyond the yield stress. AFM observations show that, at temperatures $T < 160°C$, the plastic deformation results mainly from the initiation of shear bands and their propagation through lamellae, spherulites and the whole sample. In contrast, at $T > 160°C$, AFM images exhibit spherulites which deform plastically by developing a fibrillar structure in their central part while their polar zones are undeformed.

Keywords: Atomic force microscopy; Semicrystalline polymers; Plastic deformation mechanisms

1. Introduction

The plastic deformation of bulk semicrystalline polymers is very complex, because many phenomena are likely to occur at various structural levels. The complexity arises from the specific morphology of semicrystalline polymers which consists of thin and long crystalline lamellae separated by amorphous layers; these lamellae are piled up in stacks and develop radially into spherulites. The understanding of the macroscopic mechanical behaviour of those materials requires a study of the plastic deformation mechanisms which occur at different scales—from the microscopic to the nanoscopic. Up to now, these mechanisms have been mainly studied through indirect ways, notably, X-ray diffraction and birefringence [1–6].

In contrast, with the case of single crystals and melt cast films, only very few direct observations have been made on bulk deformed samples by means of transmission electron microscopy (TEM) [7,8], by scanning electron microscopy (SEM) [9,10] or by atomic force microscopy (AFM) [11,12]. Most of the AFM experiments have been performed on ultradrawn oriented polymers to visualise and characterise the nanofibrils [11,12]; but, little effort has been made to clarify the local plastic mechanisms which are responsible for the yielding of semicrystalline polymers. In the past, Peterlin [13] has proposed a model for the transformation of crystalline lamellae into nanofibrils. This model has been derived from X-ray diffraction experiments of stretched single crystals and is often applied to stretched bulk materials. According to this model, the first steps of plastic deformation involve crystallographic processes such as intralamellar slip, twinning and phase transformation. However, twinning and phase transformation do not contribute significantly to the plastic strain [14], but rather intervene as transitory stages bringing the lamellae into an orientation more favourable for slip. In contrast to crystals of small molecules, slip can occur in a limited number of slip planes; the active slip planes must contain the chain direction since the covalent bonds of the chain backbone strongly resist the deformation. Two slip directions have been identified: (i) along the chain axis (chain slip) [4,15,16] and perpendicular to the chain axis (transverse slip) [3,17,18]. Chain slip is generally easier than the transverse slip to be activated. Crystal slip in single crystals and in bulk semicrystalline polymers is usually interpreted in terms of nucleation and propagation of dislocations [15,19–21].

In a previous study [22,23], AFM has been shown to be

* Corresponding author.

0032-3861/00/$ - see front matter
PII: S0032-3861(99)00276-1

able to characterise plasticity and damage events in isotactic polypropylene (i-PP) sheared at room temperature just beyond the yield stress and then unloaded. Mechanisms, such as cooperative kinking of lamellae parallel to the principal compressive axis or cooperative nanocracking perpendicular to the lamellae lying parallel to the principal tensile axis, have been evidenced at the lamellar scale level (20 nm). But, intralamellar slip could not be seen. We suspect that the recovery of the deformation at room temperature of the rubbery amorphous phase allows reversible crystal slip due to the entropic back stresses of the amorphous chains.

The purpose of the present paper is to show that the AFM technique is able to detect the occurrence of shear inside the lamellae and the eventual formation of shear bands. Polyamide 6 (PA6) has been chosen to carry out such a study; owing to its glassy amorphous phase at room temperature which allows quenching any deformed state before unloading. Another specificity of PA6 is the existence of intra- and intermolecular hydrogen bonds that build up a sheet-like structure along well-defined crystallographic planes. Depending of the thermal history of PA6, three kinds of crystalline structures can coexist: the monoclinic α phase, the monoclinic γ phase and the pseudo-hexagonal β phase [24–27]. The β phase is predominant in the PA6 films under investigation.

2. Experimental

2.1. PA6 films

Cast PA6 films were provided by DSM (Geelen, the Netherlands). The films, about 80 μm thick, were melted at 260°C and cooled on a chill roll at 100°C. Nucleating agents were used to speed up the crystallisation kinetics and to obtain small spherulites (diameter <5 μm). PA6 is characterised by molar weight and number average weights $M_w = 40\ 000$ g/mol and $M_n = 20\ \ 000$ g/mol. The glass transition temperature, T_g, measured by differential scanning calorimetry (DSC) is about 32°C at a relative humidity of 50%. The concentrations of α, β and γ phases were measured by Raman spectroscopy and are, respectively, equal to 11, 73 and 16% [28].

2.2. Tensile tests

The uniaxial tensile tests were performed by using an Instron tensile-test machine equipped with a temperature controlled oven. Tensile specimens with gauge dimensions 24 mm length and 5 mm wide were cut out from the films. The samples were strained up to 50%. The tests were carried out between 25 and 200°C with a strain rate $\varepsilon = 3.47 \times 10^{-2}\ s^{-1}$. For tensile tests at temperatures $T > T_g$, the samples were unloaded after the oven temperature decreased to 25°C. This procedure has been chosen in order to avoid the relaxation of the amorphous chains in the rubbery state at $T > T_g$. Because of the presence of the hydrogen bonds, PA6 is very hygroscopic; the tensile behaviour was studied for three different cases: dried films, water saturated films and films of about 50% relative humidity.

2.3. AFM experiments

All the AFM experiments were carried out in air by using a Nanoscope III Multimode microscope from Digital Instruments operating in the tapping mode (TM) [29]. In this mode, the cantilever is forced to oscillate at a frequency close to its resonance frequency with an adjustable amplitude. The tip, attached to the cantilever, was a pure silicon single crystal tip (model TSEP) with a radius of curvature of about 10 nm. The tip contacts briefly the film surface at each low position of the cantilever and the amplitude of the oscillation varies. The surface can be imaged in two different ways. “Height” images are obtained by using the feedback loop which keeps the amplitude at a constant value by translating the sample vertically with the piezoelectric scanner: height measurements are deduced from these displacements and the image reflects the topography of the surface. “Amplitude” images are obtained when the feedback loop is not connected, the amplitude can vary and the image corresponds to its variation; an “amplitude” image can be viewed as the derivative of the “height” image. To prevent indentation of the tip into the polymer surface, all the “height” images were obtained in the so-called light tapping mode with $A_{sp}/A_0 = 0.8$, where A_0 is the free oscillation amplitude and A_{sp} the set-point one [30,31]. The (512×512 pixels) images were obtained by using the (10×10 μm) piezoelectric scanner; the scanning frequency was 1 Hz and the mean value of the repulsive normal force was 0.1 nN. All the “height” images were filtered through the “Planefit” procedure. Besides the variation of the amplitude, the dephasing of the cantilever oscillation relative to the signal exciting the piezoelectric driver can be measured: that mode is called “Phase Detection Imaging” (PDI) [32] and is usually used to probe local elastic or adhesive properties at the surface. In PA6, the glassy and crystalline phases have similar elastic moduli; however, the PDI images were found to have generally better contrast than the “height” images. All the quantitative data were deduced from the “height” images, but, due to their best legibility, both “amplitude” and PDI images are shown in the present paper.

As will be shown in Section 3.1, the surface of the PA6 films is uniformly covered with spherulites. For most of them, the centre is located at the surface. Such a morphology is particularly suitable for the observation and the analysis of the plastic mechanisms by AFM; indeed, the radial lamellae lie in the film surface and the evolution of the lamellae with the plastic deformation can be easily observed. As a consequence, the native surface of PA6 films was investigated directly by AFM without any preliminary chemical treatment.

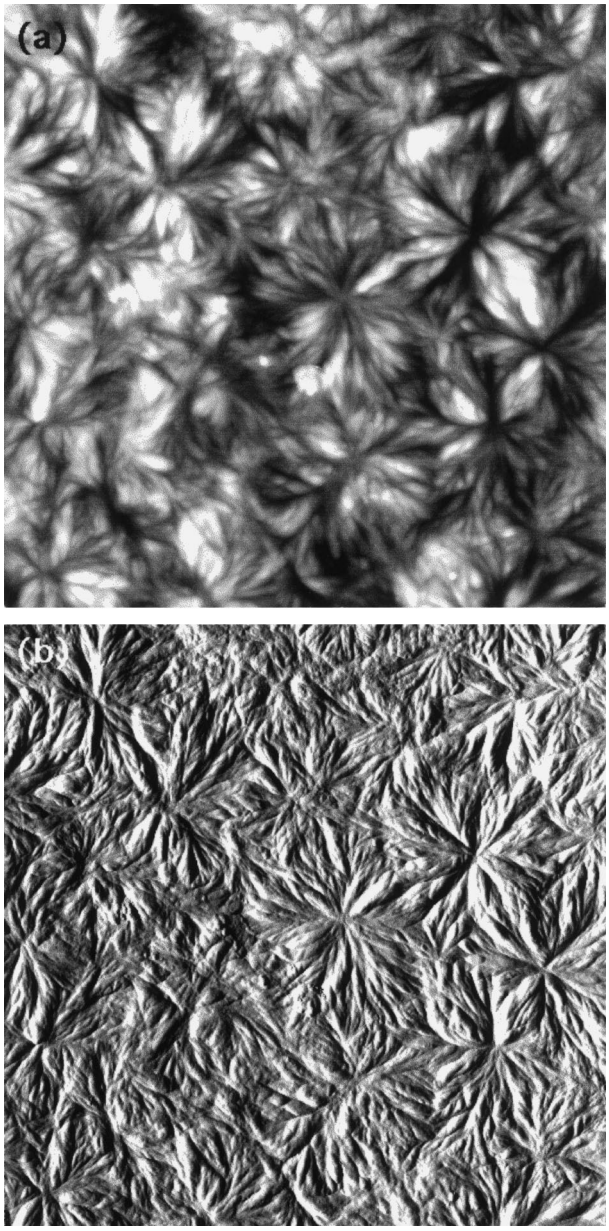

Fig. 1. An (10×10 μm) AFM image obtained on the surface of an undeformed PA6 film: a spherulitic morphology: (a) height image, *z*-range = 100 nm; (b) amplitude image.

3. Results and discussion

3.1. Morphology of undeformed samples

AFM experiments were performed on undeformed PA6 films kept at about 50% of relative humidity. Those experiments show a spherulitic morphology spreading uniformly over the whole surface of the films (Fig. 1). The mean diameter of the spherulites is 3 μm. Optical observations of ultrathin microtomised sections clearly reveal that the nucleating agents ensure a structural homogeneity through the film thickness. Details of the spherulitic morphology are shown in Fig. 2. In this (2.5×2.5 μm) image, it can be seen that the spherulites do not exhibit individual radial lamellae as in the case of polyethylene or isotactic polypropylene [22,33,34]; only lamellar bundles of about 200 nm width are observed. Even at low scale, we were unable to resolve by AFM the individual lamellae within the bundles.

The bundle-like morphology can be explained through the model proposed by Galeski et al. [35]. Due to their small width/thickness ratio (about 10 compared to 1000 in polyethylene), only three to four neighbouring lamellae may lie parallel to each other in narrow stacks [36,37]. Since small angle X-ray scattering experiments show no diffraction [38], the respective orientation of the stacks seems to be disordered. Two bundles of lamellae are shown in Fig. 3. Squares 1 and 2 are sections of the bundles perpendicular to the radial growth direction. Squares 1 contain stacks of black lamellae which have grown during the first steps of the kinetics of crystallisation. In squares 2 which exhibit black and white lamellae, the white lamellae have grown later, they join with already formed stacks or they gather themselves into new stacks. Lamellar stacks and bundles are linked together by the amorphous phase.

3.2. Plasticity mechanisms revealed by AFM in uniaxial strained PA6 films

As shown in Fig. 4, the mechanical behaviour of PA6 films depends strongly on the presence of water. It can be pointed out that the yield stress decreases with the humidity ratio while the ductility increases. This increase could be explained as follows: in the undeformed state, the water plastifies the amorphous phase (the T_g measured by DSC decreases when the humidity ratio decreases), but not the crystalline phase [39]; then, upon loading, the molecules of water go through the crystalline phase and allow the breaking of the hydrogen bonds.

In the dried state, AFM observations (Fig. 5) show that interspherulitic nanofragmentations occur at low plastic strain level (10%), both their number and size increase with increasing plastic strain; they should be responsible of the early rupture of those dried films.

Thus, to study the plastic mechanisms which occur beyond the yield point and to avoid the presence of damage, all the tensile tests were performed on the PA6 films kept in ambient air (50% of humidity). Plastic events, occurring at a given imposed plastic strain $\varepsilon = 20\%$, were studied at different scales in relation with the temperature.

3.2.1. Macroscopic scale

Fig. 6 shows three tensile specimen deformed up to 20% at temperatures $T = 25$°C (a), $T = 120$°C (b) and $T = 160$°C (c). The specimen deformed at 160°C exhibits a sharp necking, indicating that heterogeneous deformation mode takes place at temperatures $T \geq 160$°C. Below $T = 160$°C, there is no sharp necking, and the deformation is homogeneous. The observation of the surface by optical microscopy

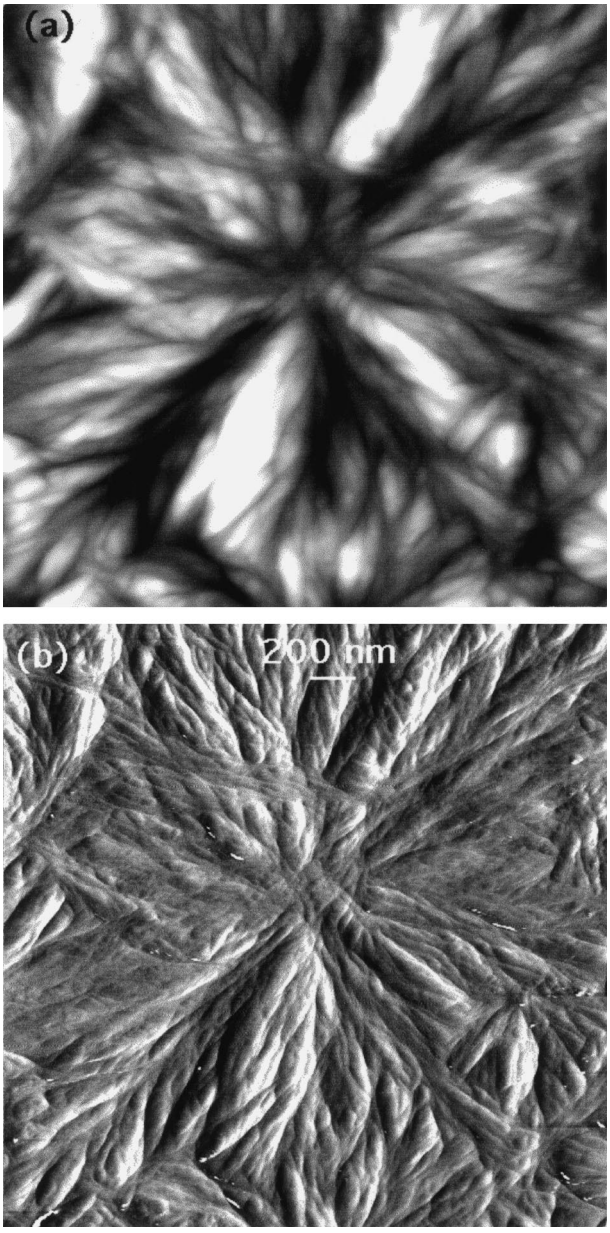

Fig. 2. Spherulitic morphology in PA6. (a) (2.5 × 2.5 μm) AFM height image, *z*-range = 0 nm; (b) phase image, phase = 25°.

or by scanning electron microscopy does not reveal any salient feature below and above T_g.

3.2.2. From the spherulitic to the lamellar scale

Again, $T = 160°C$ appears as a critical temperature. For $T \geq 160°C$, spherulites deform in a heterogeneous way. Fig. 7 shows such spherulites located in the shoulders of the neck of a sample strained at 180°C. The central part of each spherulite consists of a fibrillar structure parallel to the tensile axis. This structure is to be related to a large degree of local deformation within the spherulite along the tensile direction. The polar zones of the spherulites seem undeformed at this scale. Inhomogeneous deformation has been pointed out previously by Hay and Keller [40] (Fig. 7(c)) in

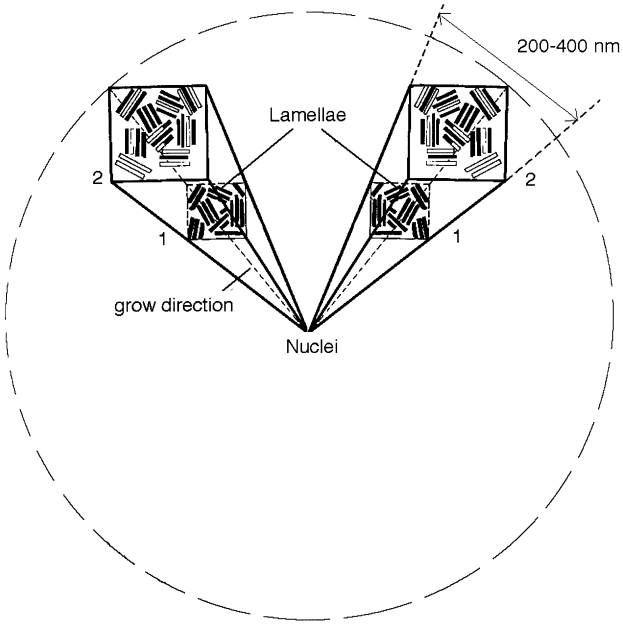

Fig. 3. Model of lamellar packing within spherulites in PA6 [34].

polyethylene films through birefringence measurements; but, such an indirect technique did not allow them to image the evolution of the spherulitic structure into fibrils between the polar zones. The heterogeneous deformation of the spherulites located at the shoulders of the neck should be responsible for the development of necking in the central part of the sample. Fig. 8 shows the morphology of the PA6 film within the neck: large fibrillar zones, perpendicular to the tensile axis, alternate with quasi undeformed areas. In the former case, there are no more spherulites while, in the latter case, undeformed spherulites can be clearly seen with some cracks running along the interspherulitic borders. In contrast, for temperatures $T < 160°C$, the deformation of the spherulite proceeds from an equiaxial to a nearly ellipsoidal shape (Fig. 9). The elongation of the spherulites along the tensile axis is thermally activated: the local deformation, which is 120% at 100°C, increases to 200% at 140°C. In addition, above T_g, AFM images (Fig. 10) reveal clearly the existence of fine parallel shear (or slip) bands which cross the spherulites and run uniformly through the whole surface of the sample. It has to be pointed out that, at a given imposed plastic strain $\varepsilon = 10\%$, no shear bands have been detected at the surface. The angle between the direction of the thin shear bands and the direction of the tensile axis is 52° whatever the temperature. In isotropic polymers such as glassy polymers, thick coarse shear bands (0.1–0.6 mm) are formed at high strain rates and intersect at 80° while thin shear bands (<1 μm) appear at low strain rates and intersect at 90° [41–44]. In the latter case, deviations from 45° have been observed in the presence of a hydrostatic component of stress [45] or in the presence of a strong elastic recovery. In our experiments, the PA6 films were quenched before unloading and any influence of elastic recovery has to be

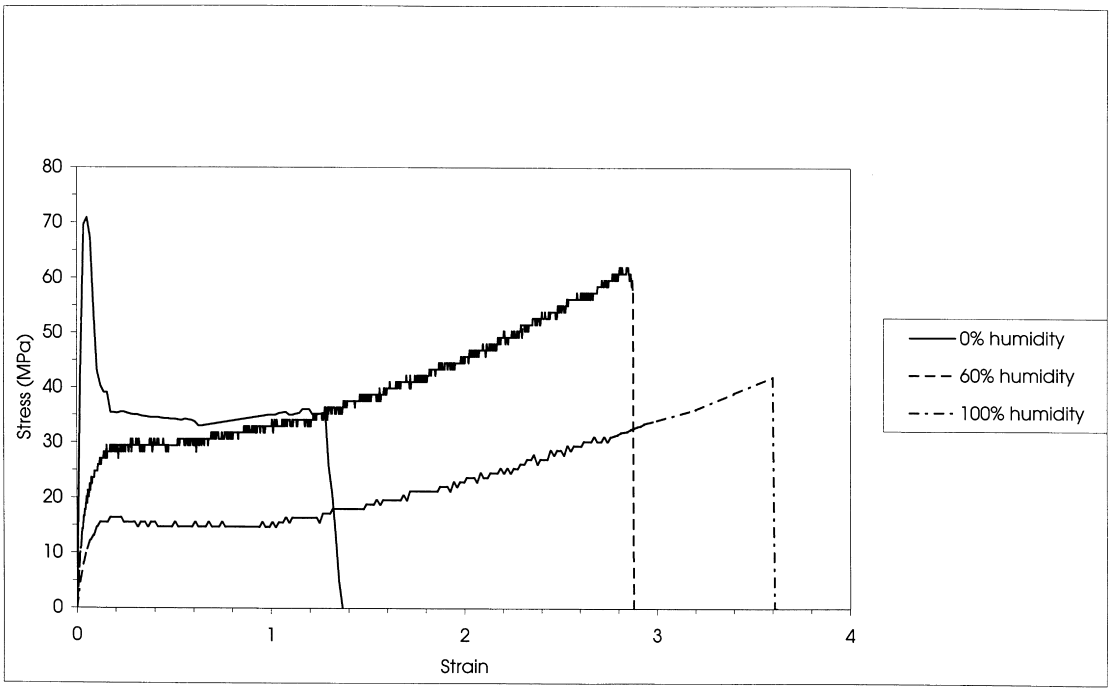

Fig. 4. Stress–strain curves of PA6 obtained at $T = 25°C$.

ruled out. On the other hand, it has been shown that the effect of a hydrostatic component of stress is to make the angle decrease from 45° [45]; here, the measured value of the angle is 52° and cannot be attributed to a pressure effect. To our knowledge, it is the first time that shear bands have been observed in semicrystalline polymers; some recent AFM observations [46] of PA11 and PA12 films, strained beyond the yield point, also show the existence of shear bands and their angle with respect to the tensile axis is greater than 45°. Up to now, the origin of such an angle is still unknown, it should not be related to the amorphous phase since the angle is not temperature-dependent, but, it could result from the crystallographic structure of the semicrystalline polymer and work is in progress to clarify this point. In contrast to the direction of the shear bands, the location and the number of shear bands depend on the temperature. Below the glass transition temperature $T_g = 32°C$, for the same imposed plastic strain, the spreading of the shear bands within the spherulites is heterogeneous. The number of shear bands per unit area is maximum near the equatorial zone and decreases regularly towards the polar zones. The difference in the propagation

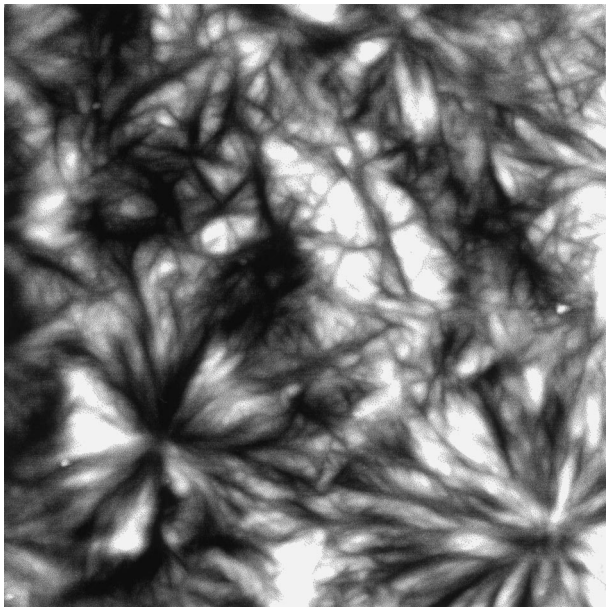

Fig. 5. PA6 film dried (0% relative humidity) and strained at $\varepsilon = 10\%$: (5×5 μm) AFM height image of the interspherulitic nanofragmentation, z-range = 40 nm. The tensile axis is vertical.

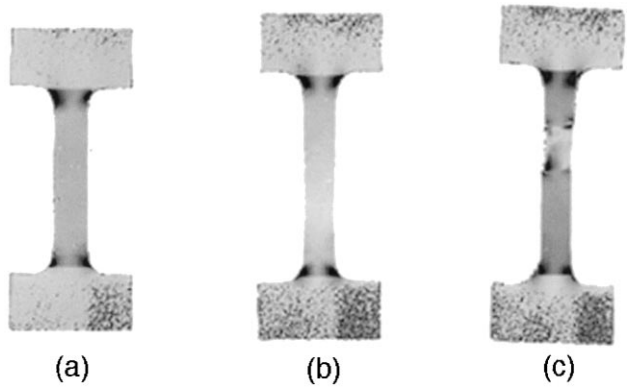

Fig. 6. Three tensile specimen deformed up to 20% at different temperatures (a) $T = 25°C$; (b) $T = 120°C$ and; (c) $T = 160°C$.

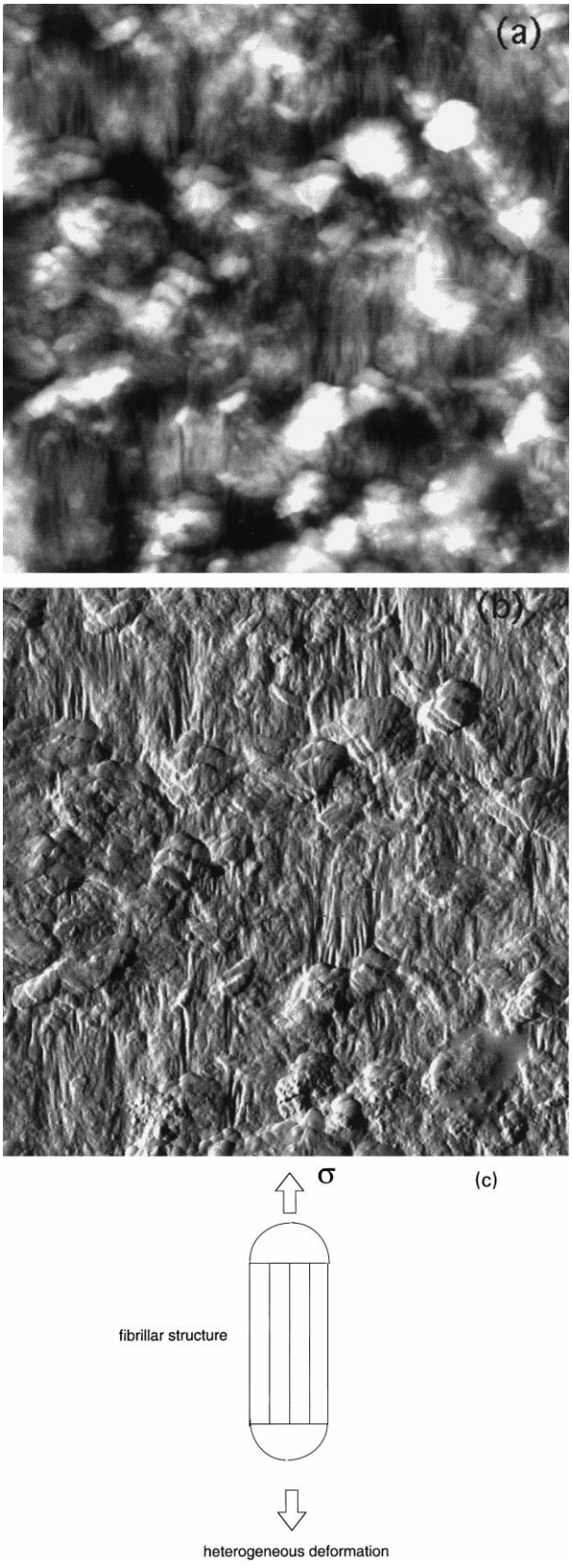

Fig. 7. AFM image (14 × 14 μm) of the spherulites located in the shoulders of the neck of a sample strained at 180°C: Inhomogeneous deformation (a) height image, z-range = 100 nm; (b) amplitude image; (c) schema of a spherulite deformed heterogeneously. The tensile axis is vertical.

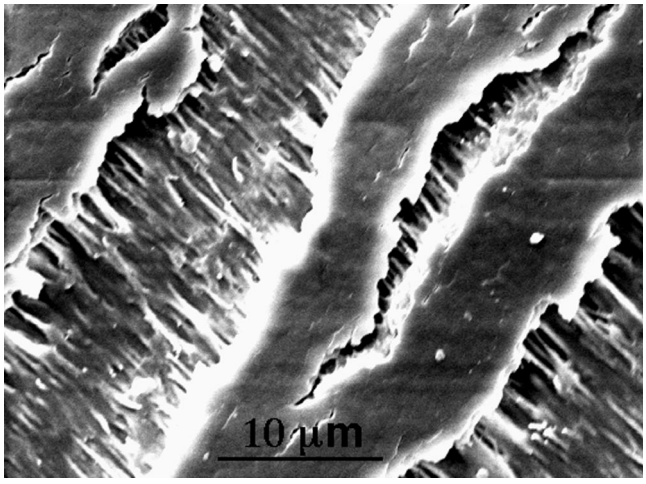

Fig. 8. SEM image of the morphology of the PA6 film within the neck. The tensile axis is perpendicular to the crack direction.

of shear bands above and below T_g could be explained as follows: above T_g, the amorphous phase behaves as an elastomer, interlamellar shear is easy and makes possible the rotation of the lamellae; Jolly et al. [47] have shown that, at low strains, all the lamellae rotate towards the direction which favours intralamellar slip at moderate strains. In contrast, below T_g, the amorphous phase is glassy and interlamellae shear is more difficult, thus, only the lamellae whose direction is favourable to the intralamellar slip will be sheared.

Fig. 11 shows a 3D view of a sheared lamella ($T < T_g$). In contrast with the surface of an undeformed lamella, the surface of a sheared one exhibits equidistant ridges (3–4 nm): each shear band crosses the lamella between two consecutive ridges. As mentioned above, the number and the width of the shear bands is temperature-dependent. Our future work is to make quantitative studies of this dependence.

Except in some undeformed polar zones, individual lamellae or stacks of 3 or 4 edge-on lamellae can be clearly seen in any area of the spherulites. Thus, because of the applied tensile stress, the bundles of lamellae, observed in the undeformed state (Fig. 2), have been untangled: locally, the tensile stress leads to interlamellar shear and/or separation which both allow the rotation of the lamellae [47]. The lamellar thickness can be deduced from the observation of edge-on lamellae. In the areas crossed by the shear bands, it has not been possible to measure accurately the lamellar thickness due to the presence of these shear bands. The lamellar thickness has been measured in polar zones such as the one shown in Fig. 12. The lamellae are crossed by nanocracks; but, the distance between the nanocracks is rather large and the mean lamellar thickness has been deduced from measurements over distances of about 60 nm along the radial direction. Fig. 13 shows a 2D section along an axis perpendicular to the lamellar direction: the thickness value 7 ± 1 nm is in agreement with previous

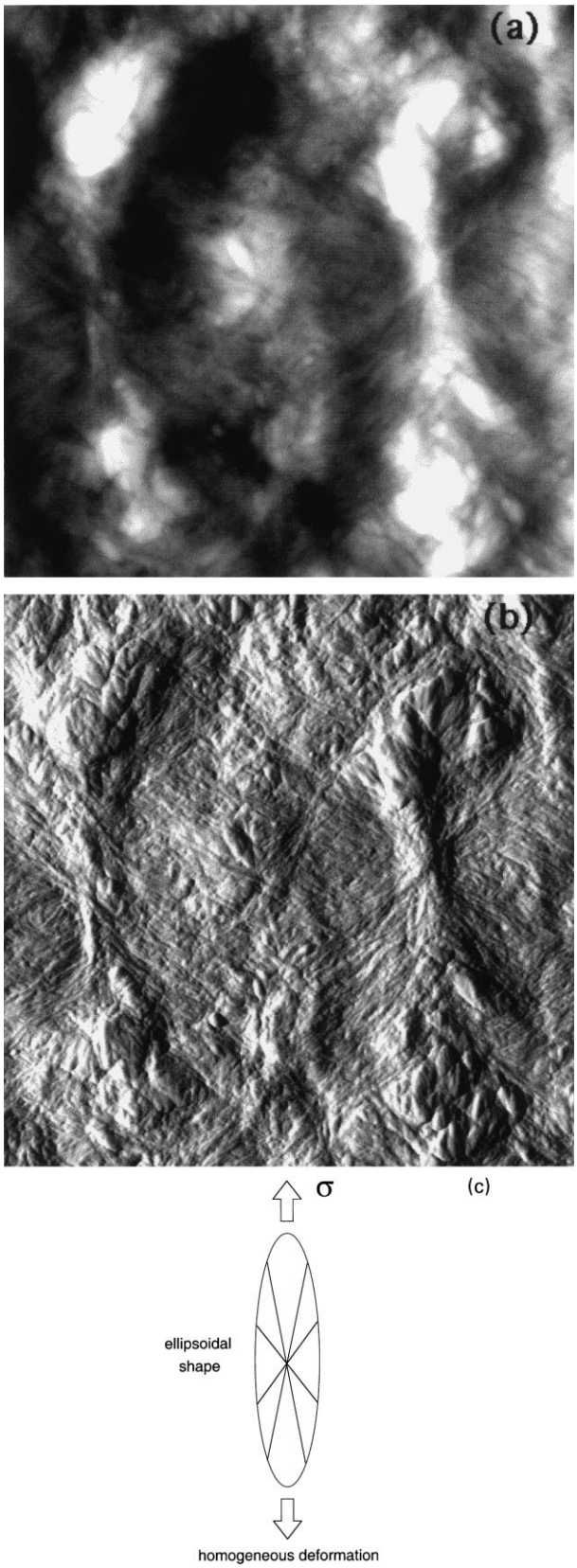

Fig. 9. AFM image (10×10 μm) of two spherulites after a macroscopic deformation of 20% at $T = 120$°C. (a) height image, z-range = 75 nm; (b) amplitude image; (c) schema of a spherulite deformed homogeneously. The tensile axis is vertical.

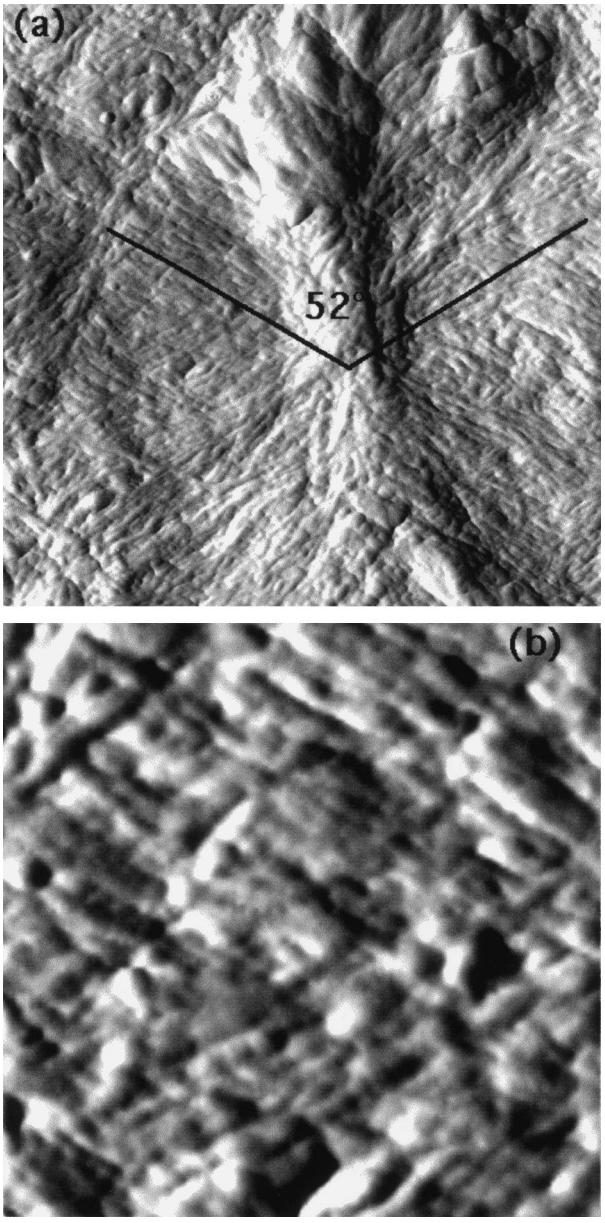

Fig. 10. Fine parallel shear (or slip) bands cross the spherulite with an angle with the tensile axis of 52° (a) (2.5×2.5 μm) AFM amplitude image (b) (700×700 nm) AFM amplitude image. The tensile axis is vertical.

data [35,36]. In polar zones, the direction of growth, *a*, of the lamellae [35,48] is almost parallel to the tensile axis; thus, the nanocracks, which run perpendicularly through the lamellae, lie in (100) planes. The presence of such nanocracks could result from the interlamellar shear of the amorphous phase which entails the stretching of tie and bridging molecules and thus leads to stress concentrations in some (100) planes of the lamellae. The number of nanocracks increases with the imposed plastic strain.

At present, these preliminary data, obtained at the lamellar level, do not allow us to conclude about the nature of the crystal slip systems involved in the plastic deformation. Such a study is planned in the near future. In the past,

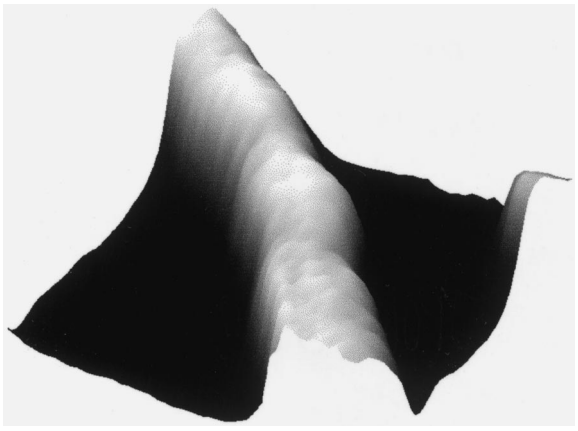

Fig. 11. 3D view of a sheared lamella when $T < T_g$. AFM phase image, phase = 10°.

most of the studies on the plastic deformation of PA6 have dealt with the α phase which is the more stable phase. In the α phase, the hydrogen bonds are formed in the zigzag (001) planes and between antiparallel chains [24]; previous studies on monocrystals have shown that the slip planes are observed only parallel to the H-bonds (001) sheets [49]. In the PA6 films under study, the pseudo-hexagonal β(phase is predominant; but the structure of this phase, which appears as partially disordered from the X-ray diffraction patterns [50], is much less known than that of the α phase. The structure of the β phase has been mainly studied in melt spun fibers; but, the X-ray data are explained in different ways. Ziabicki [51] proposed a model of structure in which chains with a repeating distance of 0.86 nm per monomeric unit are packed in a pseudo-hexagonal lattice with $a = 0.48$ nm and are randomly rotated around

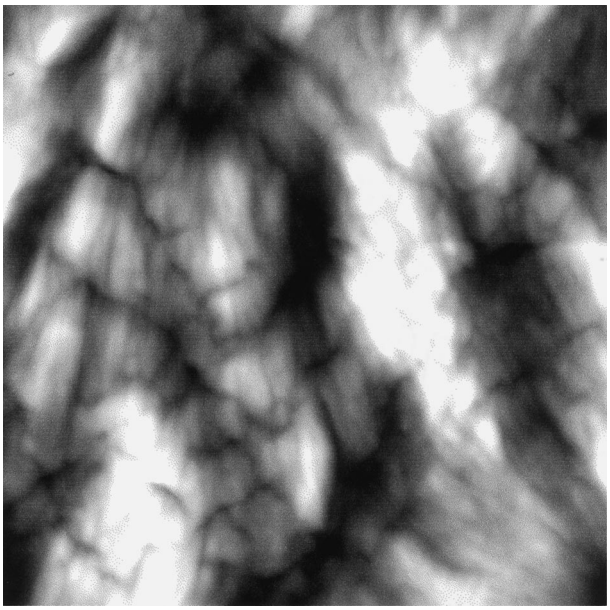

Fig. 12. Lamellae crossed by nanocracks in polar zones. (2 × 2 μm) AFM height image, *z*-range = 30 nm. The tensile axis is vertical.

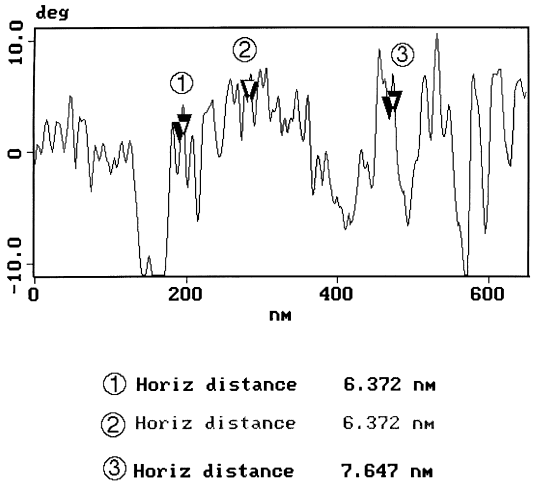

Fig. 13. 2D section of an AFM phase image ($A_{sp}/A_0 \approx 0.5$) along an axis perpendicular to the lamellar direction.

the chain axis; the hydrogen bonds form in all directions, as a consequence. Stepaniak et al. [24] suggested that the β phase could be described as a "pleated" α phase. The expected slip planes in PA6 are the (100) and (001) planes, the chain slip direction is the [010] direction; by studying the active slip systems by AFM, we expect to be able to determine what structure among all the proposed models is compatible with the observed plastic deformation.

4. Conclusion

We have shown that atomic force microscopy is a good tool to image directly the plastic events which occur from the spherulitic scale to the lamellar one in polyamide 6 films. Under uniaxial tension, beyond yielding, PA6 films exhibit, at the macroscopic scale, a sharp necking at temperatures higher than 160°C, while the plastic deformation is homogeneous below 160°C. AFM observations show that, above 160°C, in the shoulders of the neck, the central part of each spherulite consists of a fibrillar structure parallel to the tensile axis and the polar zones of the spherulites seem undeformed. In contrast, below 160°C, the plastic deformation proceeds mainly by shear banding: above T_g, intralamellar shear makes possible the rotation of the lamellae at low strains and, at intermediate strains, shear bands cross the crystalline lamellae, the spherulites and run uniformly through the whole surface of the sample; below T_g, interlamellar shear is more difficult and the propagation of shear bands is more heteregeneous. Whatever the temperature, shear bands intersect at an angle of 104°.

Our next aim is to focus attention on the lamellar scale in order to identify the active slip systems, then, to investigate the homogeneous or heterogeneous character of the crystal slip and, finally, to interpret our data in terms of nucleation and propagation of dislocations in the crystalline phase.

Acknowledgements

The authors are very grateful to B. Escaig (LSPES, USTLille, France) and to B. Lotz (ICS, Strasbourg, France) for several illuminating discussions. This research was supported in part by the Contrat Plan Etat-Région 1994–1999, by the FEDER (CEE Program) and by the Ministère de l'Enseignement Supérieur et de la Recherche.

References

[1] Young RJ, Bowden PB, Ritchie JM, Rider JG. J Mater Sci 1973;8:23.
[2] Pope DP, Keller AJ. J Polym Sci: Polym Phys Ed 1974;12:145.
[3] Lin L, Argon AS. Macromolecules 1992;25:4011.
[4] Gaucher-Miri V, François P, Séguéla R. J Polym Sci Polym Phys Ed 1996;34:1113.
[5] Hay IL, Keller A. Kolloid-Z Z-Polym 1965;204:43.
[6] Weynant E, Haudin JM, G'Sell C. J Mater Sci 1980;15:2677.
[7] Bartzack Z, Cohen RE, Argon AS. Macromolecules 1992;25:4692.
[8] Bartzack Z, Argon AS, Cohen RE. Macromolecules 1994;35:3427.
[9] Dahoun A, Aboulfaraj M, G'Sell C, Molinari A, Canova GR. Polym Engng Sci 1995;35:317.
[10] Aboulfaraj M, G'Sell C, Ulrich B, Dahoun A. Polymer 1995;36:731.
[11] Snétivy D, Vancso GJ. Polymer 1994;35:461.
[12] Cramer K, Schneider M, Mulhaupt R, Cantow HJ, Magonov SN. Polym Bull 1994;32:637.
[13] Peterlin A. J Mater Sci 1971;6:490.
[14] Bowden PB, Young RJ. J Mater Sci 1974;14:2034.
[15] Gleiter H, Argon AS. Phil Mag 1976;24:71.
[16] Gaucher-Miri V, Séguéla R. Macromolecules 1997;30:1158.
[17] Franck FC, Keller A, O'Connor A. Phil Mag 1958;3:64.
[18] Keller A. J Polym Sci 1956;21:363.
[19] Petermann J, Gleiter H. J Mater Sci 1972;8:673.
[20] Young RJ. Phil Mag 1974;30:85.
[21] Shadrake LG, Guiu F. Phil Mag 1976;34:565.
[22] Castelein G, Coulon G, G'Sell C. Polym Engng Sci 1997;37:1694.
[23] Coulon G, Castelein G, G'Sell C. Polymer 1998;40:95.
[24] Stepaniak RF, Garton A, Carlsson DJ, Wiles DM. J Polym Sci: Polym Phys Ed 1979;17:987.
[25] Holmes DR, Bunn CW, Smith DJ. J Polym Sci 1955;17:159.
[26] Arimoto H. J Polym Sci: Polym Phys Ed 1992;30:489.
[27] Ishida H, Rotter G. J Polym Sci A 1967;2-5:939.
[28] Ferreiro V, et al. Submitted for publication.
[29] Digital Instruments, Nanoscope III, Scanning Probe Microscopes, Instruction Manual, Santa Barbara, CA: Digital Instruments.
[30] Bar G, Thomann Y, Brandsch R, Cantow HJ. Langmuir 1997;13:3807.
[31] Brandsch R, Bar G. Langmuir 1997;13:6349.
[32] Magonov SN, Whangbo MH. Surface analysis with STM and AFM, Weinheim: VCH, 1996.
[33] Zhou H, Wilkes GL. Polymer 1997;38:5735.
[34] Varga J. J Mater Sci 1992;27:2557.
[35] Galeski A, Cohen RE. Makromol Chem 1986;188:1195.
[36] Atkins EDT, Hill MJ. Polymer 1995;36:35.
[37] Atkins EDT, Keller A. J Polym Sci: Polym Phys Ed 1972;10:863.
[38] Séguéla R. Unpublished data.
[39] Galeski A, Cohen RE. Macromolecules 1988;21:2761.
[40] Hay IL, Keller A. J Mater Sci 1967;2:538.
[41] Li JCM. Polym Engng Sci 1984;24:750.
[42] Whitney W, Andrews RD. J Polym Sci C 1967;16:2981.
[43] Wu JBC, Li JCM. J Mater Sci 1976;11:434.
[44] Bowden PB, Raha S. Phil Mag 1970;22:463.
[45] Escaig B. Polym Engng Sci 1997;37:1641.
[46] Pennec Y. Unpublished data.
[47] Jolly L, Tidu A, Heizmann JJ, Dal Maso F. JEPO XXV, La Colle-sur-Loup, France, 1997.
[48] Wittmann JC, Lotz B. J Polym Sci 1985;23:200.
[49] Zaukelies DA. J Appl Phys 1962;9:2797.
[50] Penel-Pierron L, Depecker C, Lefebvre J-M, Séguéla R. In: International Symposium on Orientation of Polymers, Boucherville, Quebec, Canada, September 23–25, 1998.
[51] Ziabicki VA. Kolloid-Z Z-Polym 1959;167:132.